Scientific paper

Quasi-static and Dynamic Mechanical Properties of Engineered Geopolymer Composites with Hybrid PVA and Recycled Steel Fibres

Hui Zhong[1], Yi Wang[2] and Mingzhong Zhang[3*]

Received 12 November 2022, accepted 30 April 2023 doi:10.3151/jact.21.405

Abstract

Recycled tyre steel (RTS) fibre is favoured as a replacement for industrial steel fibre to reduce the environmental impact and material cost of fibre reinforced cementitious composites as well as a potential substitute for the commonly used polyvinyl alcohol (PVA) fibre to develop sustainable engineered geopolymer composites (EGC). This paper systematically examines the effect of hybrid PVA and RTS fibre dosage on the engineering properties of fly ash-slag based EGC, with special focus on uniaxial tensile behaviour and dynamic compressive and splitting tensile behaviour. Results indicate that combining RTS fibres with PVA fibres can effectively improve the drying shrinkage resistance of EGC. All studied EGC mixes exhibit expected strain-hardening and multiple cracking behaviour under uniaxial tension and about 5% enhancement in tensile strength is captured for EGC when 0.25% PVA fibre is replaced with RTS fibre. The incorporation of RTS fibres can improve the quasi-static compressive strength of EGC up to 31%, as compared to EGC with 2.0% PVA fibre. Replacing 0.25 to 0.5% PVA fibre with RTS fibre is beneficial to the dynamic mechanical properties of EGC, where up to 20% improvement in dynamic splitting tensile strength is found for EGC.

1. Introduction

Concrete is the most widely used construction material, which is inherently brittle and prone to cracking. To mitigate these issues, fibre reinforced cementitious composites (FRCC) have been developed by incorporating several types of short fibres. As a special class of FRCC, engineered cementitious composites (ECC) exhibit superior crack resistance and ultra-high tensile strain capacity beyond 2% which is much greater than that of plain concrete (i.e., 0.01%) (Li 2019). ECC also has unique tensile strain-hardening behaviour along with stable microcrack propagation with an average crack width below 100 μm. Given these characteristics, ECC outperforms other materials in engineering applications, such as hydraulic structures requiring tight crack widths, retrofitting projects for longer service life, and seismic resilient buildings (Paulay and Binney 1974; Rokugo *et al.* 2009; Rokugo and Kanda 2013).

The typical ECC contains approximately 2 to 3 times higher Portland cement content than normal concrete due to the absence of coarse aggregates (Wang and Li 2007), which would lower its greenness and sustainability as the manufacture of Portland cement consumes a huge amount of natural resources (e.g., limestone) and requires extensive energy consumption as well as contributing to around 8% of the global CO_2 emissions (Luukkonen *et al.* 2018). Thus, finding alternative sustainable binding materials for ECC is urgently needed. Given the better engineering properties, superior thermal performance, reduced greenhouse emissions and low energy consumption, geopolymers made from industrial by-products such as fly ash and ground granulated blast-furnace slag are considered as a promising alternative to Portland cement, which can reduce energy consumption and carbon footprint by 40 to 80% (Provis and Van Deventer 2009). In recent years, engineered geopolymer composites (EGC) have been developed by combining the benefits of geopolymers and ECC (Zhong and Zhang 2023). To date, different types of precursors have been used to synthesise EGC and among them, blended fly ash and slag is increasingly adopted as the resultant composites can achieve a good synergy between fresh and hardened properties under ambient temperature, which cannot be attained by the composites made with either fly ash or slag solely (Nematollahi *et al.* 2017a, 2017b; Zhang *et al.* 2020b; Zhong and Zhang 2021; Wang *et al.* 2022).

Similar to ECC, hydrophilic polyvinyl alcohol (PVA) with oil coating or hydrophobic polyethylene (PE) fibres have been frequently used as fibre reinforcement in EGC for the desired tensile strength and ductility. Nevertheless, their material costs and potential environmental impacts whilst manufacturing would lower the sustainability of EGC and limit its widespread engineering applications (Yu and Leung 2017; Merli *et al.* 2019; Zhang *et al.* 2020a). Previous studies found that about 70 to 80% of the total material cost of ECC and EGC comes from PVA fibres (Yu and Leung 2017; Zhong and Zhang 2021). The

[1]Ph.D Student, Department of Civil, Environmental and Geomatic Engineering, University College London.
[2]Post-doctoral Researcher, Department of Civil, Environmental and Geomatic Engineering, University College London.
[3]Associate Professor, Department of Civil, Environmental and Geomatic Engineering, University College London.
*Corresponding author,
E-mail: mingzhong.zhang@ucl.ac.uk

Table 1 Chemical compositions (wt.%) of fly ash and slag.

Oxide	SiO_2	Al_2O_3	CaO	MgO	K_2O	Fe_2O_3	TiO_2	Na_2O	SO_3	LOI
Fly ash	57.02	32.35	2.88	0.58	2.07	3.01	1.26	0.03	0.41	0.39
Slag	31.85	17.31	41.20	6.13	0.33	0.34	0.62	0.03	1.78	0.41

cost of PE fibres is even around 8 times higher as compared with PVA fibres (Li 2008). Hence, an increasing number of studies have recently focused on the usage of lower cost and more sustainable fibres including recycled fibres to develop either ECC or EGC.

Regarding ECC, most studies have employed recycled polyethylene terephthalate (PET) fibres to replace PVA fibres (Choi *et al.* 2012; Lu *et al.* 2018; Yu *et al.* 2018), revealing that the total material cost and sustainability indicators especially embodied energy were reduced in the presence of recycled PET fibres. Nevertheless, the uniaxial tensile behaviour of the resultant composites dropped with the increasing content of recycled PET fibres. To reduce the increasing landfill burden of end-of-life tyres, a few studies have explored the feasibility of using recycled tyre fibres such as polymer and steel fibres to partially substitute PVA fibres in EGC. Adopting recycled tyre polymer (RTP) fibre at 0.25 to 0.5% (by volume) to replace PVA fibre was beneficial to the dynamic mechanical properties of EGC and the material cost and embodied energy dropped by about 35% and 16%, respectively, when the RTP fibre substitution content was 1.0% (Zhong and Zhang 2021, 2022a, 2022b). Incorporating recycled tyre steel (RTS) fibres in EGC also has a great potential to improve its overall engineering properties along with cost-effectiveness and sustainability as many existing studies proved the benefits of RTS fibres in ordinary concrete (Liew and Akbar 2020). A previous study found that EGC containing RTS fibres had about 26% higher compressive strength and 73% lower drying shrinkage in comparison with EGC reinforced with 2.0% PVA fibre (Wang *et al.* 2020). Although the flexural strength of EGC was not improved when PVA fibres were partly substituted with RTS fibres, the crack width after flexural loading was narrowed down, which is consistent with a previous study (Lao *et al.* 2022) that the good bonding between normal steel fibres and the geopolymer matrix resulted in a very fine crack width (10 to 20 μm) for the resultant composites. It is worth noting that the specimen presenting deflection-hardening behaviour may not mean it could exhibit strain-hardening performance under uniaxial tension (Li 2019). Hence, it is important to understand the effect of RTS fibre on the uniaxial tensile behaviour of EGC to further explore its feasibility in EGC, which has not been addressed yet. In addition, concrete structures may experience both static and dynamic loadings during the service life, implying that it is also essential to understand the dynamic mechanical properties of EGC containing RTS fibres to promote its widespread application.

The main purpose of this paper is to systematically investigate the engineering properties of fly ash-slag based EGC reinforced with hybrid PVA and RTS fibres under ambient curing, with special focus on the uniaxial tensile behaviour and dynamic mechanical properties. A series of tests were first conducted to measure workability, drying shrinkage, uniaxial tensile behaviour, and quasi-static compressive strength. Afterwards, a split Hopkinson pressure bar (SHPB) was employed to explore the effects of strain rate and fibre on the dynamic compressive behaviour of EGC in terms of failure pattern, stress-strain response, dynamic compressive strength, energy absorption capacity, and dynamic increase factor (DIF). Moreover, the failure pattern and dynamic splitting tensile strength of EGC under various impact velocities were examined. Based on the obtained experimental data, the underlying mechanisms were discussed in depth.

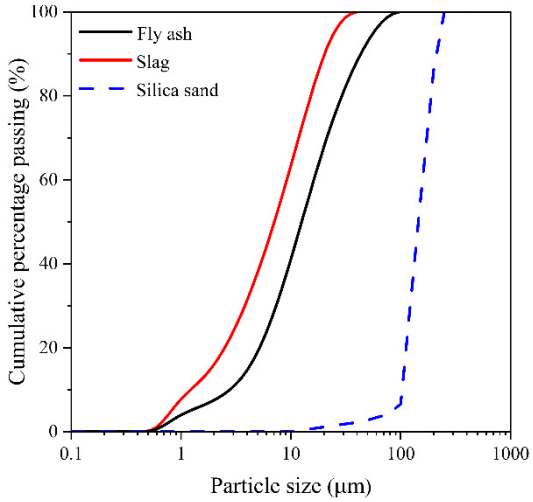

Fig. 1 Particle size distribution of fly ash, slag, and silica sand.

2. Experimental program

2.1 Raw materials

Low calcium fly ash equivalent to Class F fly ash as per ASTM C618-17a (ASTM 2017b) and ground granulated blast-furnace slag were adopted as the precursors to synthesise EGC, the chemical composition and particle size distribution of which are given in **Table 1** and **Fig. 1**, respectively. Micro silica sand with a specific gravity of 2.66 was used as fine aggregate and its particle size is also presented in **Fig. 1**. The sodium silicate solution with a modulus (SiO_2/Na_2O) of 2.0 was mixed with 10 M sodium hydroxide solution to produce the alkaline activator. 10 M sodium hydroxide solution was obtained by dissolving 400 g of sodium hydroxide powders in 1 L of tap water. A small amount of polycarboxylate-based superplasticiser (SP) was added to improve the workability and fibre dispersion of EGC. The solid content of the used SP was around 35%.

Table 2 Properties of PVA and RTS fibres.

Fibre type	Length (mm)	Diameter (μm)	Density (g/cm^3)	Tensile strength (MPa)	Elastic modulus (GPa)
PVA	12	40	1.3	1600	41
RTS	12.8*	220	7.8	2165	200

*Average length.

Table 3 Mix proportions of EGC.

Mix ID	Binder		Activator/binder	Sand/binder	SP/binder	PVA (vol%)	RTS (vol%)
	Fly ash	Slag					
P1.5	0.8	0.2	0.45	0.2	0.01	1.5	0
P2	0.8	0.2	0.45	0.2	0.01	2.0	0
P1.75R0.25	0.8	0.2	0.45	0.2	0.01	1.75	0.25
P1.5R0.5	0.8	0.2	0.45	0.2	0.01	1.5	0.5

In this study, the geopolymer matrix was either reinforced with PVA fibres or the combination of PVA and RTS fibres, the main properties and physical appearance of which are illustrated in **Table 2** and **Fig. 2**, respectively. PVA fibres with 1.2 wt.% oil coating were supplied by Kuraray Co., Ltd., Japan. It should be noted that the as-received RTS fibres had lengths ranging from 2 mm to 27 mm, which need to be screened to avoid the adverse effect on the fresh and hardened properties of the resultant composites. It was reported that the strength of steel fibre reinforced cementitious composites was lower when the length of the incorporated RTS fibres was mostly less than 9 mm (Isa *et al.* 2020). In addition, the preliminary results from a previous study (Zhong *et al.* 2023) indicated that the mixture containing RTS fibres with length between 9 mm and 16 mm can exhibit better quasi-static compressive, flexural and tensile strengths compared to mixes containing RTS fibres with other length ranges (4 to 9 mm and 16 to 24 mm). It should be noted that the adopted RTS fibres in this study were the same as those in this previous study. Thus, RTS fibres with a length range of 9 to 16 mm and an average length of around 12.8 mm were used in this study (see **Fig. 2**).

2.2 Mix proportions

Table 3 lists the mix proportions of EGC studied herein, where the fly ash/slag ratio, activator/binder ratio, and sand/binder ratio were kept constant as 4.0, 0.45, and 0.2, respectively (Wang *et al.* 2022). The dosage of SP was set as 1.0% of the total binder mass for all mixtures. For the meaning of mix ID, 'P1.5' denotes the mix with 1.5% PVA fibre while P1.75R0.25 stands for the mixture containing 1.75% PVA fibre and 0.25% RTS fibre.

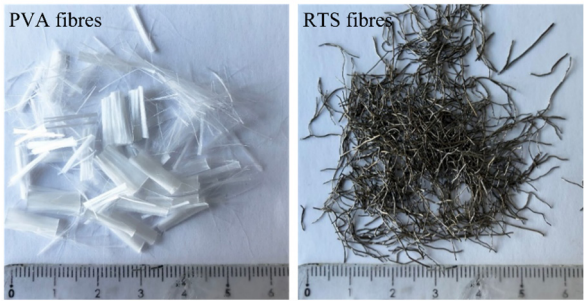

Fig. 2 Physical appearance of PVA and RTS fibres.

2.3 Specimen preparation

All EGC mixtures here were prepared using a Hobart mixer under an ambient temperature. The adopted mixing procedure was consistent with that employed in a previous study (Wang *et al.* 2022). Firstly, a homogenous dry mix was attained by adding fly ash, slag and silica sand into the mixer and mixing for 1.5 min. Subsequently, the alkaline activator was slowly added into the dry mix and mixed for around 3 min. Afterwards, SP was added and mixed for another 1 min. PVA fibres were then evenly incorporated into the wet mix, followed by the slow and careful addition of RTS fibres (if any). Once all fibres were well dispersed in the mixture, the whole mixture was mixed for another 1 min. The total mixing time lasted for around 10 min. After that, the fresh EGC was immediately poured into the moulds with sufficient vibration to remove the air bubbles. All samples were de-moulded after 24 h and then cured in a standard room with temperature of 20±2°C and relative humidity of 95% until 28 d (except for samples prepared for drying shrinkage tests).

2.4 Testing methods

2.4.1 Workability test

As per ASTM C1437-15 (ASTM 2015), the flow table test was carried out to measure the spread diameters of fresh EGC mixtures in two directions. The flow of each mixture can be calculated as:

$$\text{Flow} = \frac{D - D_0}{D_0} \times 100\% \quad (1)$$

where D is the average spread diameter of the fresh EGC and D_0 represents the bottom diameter of the flow table mould (100 mm).

2.4.2 Drying shrinkage test

The drying shrinkage test was performed according to ASTM C490-17 (ASTM 2017a). The samples were cast into 50×50×280 mm prismatic moulds when the mixing

procedure ended. The first comparator reading was recorded for each mix immediately after the de-moulding and all specimens were then placed in an environment with temperature of 20±2°C and relative humidity of 60±5%. The subsequent comparator readings at various ages were recorded and compared with the initial reading to determine the drying shrinkage.

2.4.3 Quai-static uniaxial tension test

Dog-bone shaped specimens with a cross-sectional area of 13×30 mm and a total length of 330 mm were fabricated for uniaxial tensile tests (JSCE 2008), as illustrated in **Fig. 3(a)**. All dog-bone shaped samples were inserted into a testing mould as in **Fig. 3(b)** and a uniaxial tensile load was applied at a constant loading rate of 0.5 mm/min. Two linear displacement transducers (LVDTs) were installed around the gauge part of the test specimen to measure the tensile deformation whilst testing. The tensile strain was calculated by dividing the tensile deformation by the gauge length of the sample (80 mm).

2.4.4 Quasi-static compression test

According to ASTM C109/C109M-20b (ASTM 2020), the quasi-static compressive strength test was conducted on cubic EGC samples (50×50×50 mm) using a universal testing machine. The constant loading rate of 1200 N/s was employed for all test samples.

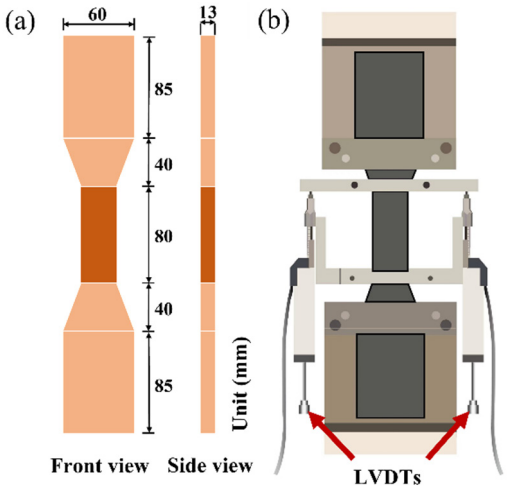

Fig. 3 Schematic illustration of (a) dog-bone shaped sample, and (b) setup for uniaxial tensile test.

2.4.5 Split Hopkinson pressure bar test

The dynamic compressive behaviour of EGC was investigated using a 100-mm diameter SHPB testing apparatus, as shown in **Fig. 4**. The details of this SHPB testing system can be found in previous studies (Chen *et al.* 2019; Zhong and Zhang 2022b). EGC specimens were cast into ø100×50 mm cylindrical moulds and adopting this sample size can reduce the axial inertia effect during the impact loading (Bertholf and Karnes 1975; Khan *et al.* 2018). All test samples were sandwiched between the incident bar and the transmission bar, and the loading surfaces of the samples were covered by some grease to mitigate the end friction effect. The impact velocity can be adjusted by either varying the depth of the striker or altering the pressure level. In this study, the employed impact velocities were about 6 ms^{-1}, 8 ms^{-1} and 10 ms^{-1}, which were selected to study the dynamic mechanical properties of EGC from slight damage to severe fragmentation corresponding to different loading conditions in the real world. When the striker impacted the incident bar, three pulses (ε_i, ε_r and ε_t) were generated and then collected by the strain gauges mounted on the incident and transmission bars. According to one-dimensional elastic stress wave theory, the history of compressive stress $\sigma_{dc}(t)$, compressive strain ε_{dc}, and strain rate $\dot{\varepsilon}(t)$ can be determined as follows (Chen and Song 2011):

$$\begin{cases} \sigma_{dc}(t) = \dfrac{E_1 A_1}{2A_2}\left(\varepsilon_i(t) + \varepsilon_r(t) + \varepsilon_t(t)\right) \\ \varepsilon_{dc}(t) = \dfrac{C_1}{l_2}\displaystyle\int_0^t \left(\varepsilon_i(t) - \varepsilon_r(t) - \varepsilon_t(t)\right)dt \\ \dot{\varepsilon}(t) = \dfrac{C_1}{l_2}\left(\varepsilon_i(t) - \varepsilon_r(t) - \varepsilon_t(t)\right) \end{cases} \quad (2)$$

where E_1, A_1 and C_1 are the elastic modulus, cross-sectional area and wave propagation velocity of the bar, respectively, and A_2 and l_2 denote the cross-sectional area and length of the EGC sample, respectively.

The dynamic splitting tensile strength (f_{dt}) of EGC under various impact velocities was also characterised using the SHPB apparatus (Khan *et al.* 2019; Lai *et al.* 2022), which can be calculated as:

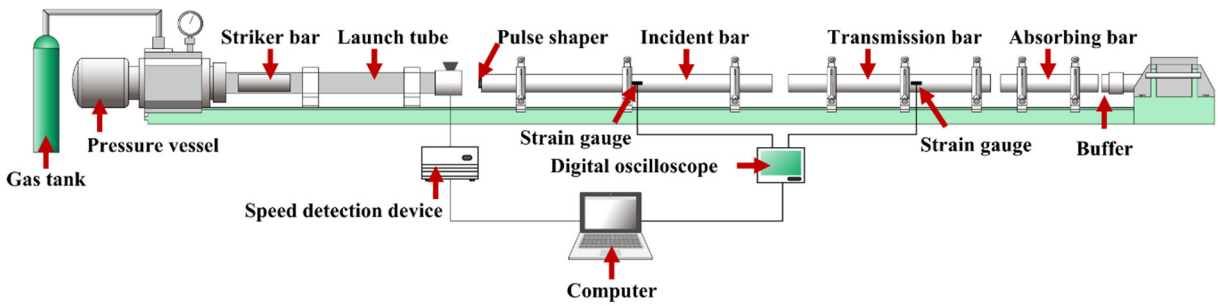

Fig. 4 Schematic diagram of SHPB testing apparatus (Zhong and Zhang 2022b).

$$f_{dt} = \frac{2F_{dt}}{\pi D_2 l_2} \quad (3)$$

where F_{dt} is the splitting tensile force acting on the EGC specimen which can be derived from Eq. (2), and D_2 stand for the diameter of the test sample.

3. Results and discussion

3.1 Workability

Figure 5 shows the flow values of all EGC mixtures with various fibre dosages. A large flow value indicates better workability, allowing easier casting and compaction. Increasing either PVA or RTS fibre content reduced the flow value of EGC due to the increased interaction between fibres and fibres and the matrix and the decreased packing density (Ranjbar and Zhang 2020). As compared with P2, the flow values of EGC containing RTS fibres were 2.50% and 4.76% lower, consistent with a previous study (Wang *et al.* 2020). Different from the effect of mono-fibre reinforcement on the workability of composites, the mutual effect between hybrid fibres can affect the flowability of the matrix by restricting each other's rotation (Yu *et al.* 2014). RTS fibres with ununiform lengths and deformed shapes can increase the possibility of inducing a congested fibre network and thereby, reducing the overall flowability. However, the smaller aspect ratio (mostly 65) of RTS fibres can compensate for the workability loss mentioned above. Thus, the observed reductions here caused by the presence of RTS fibres were insignificant and were much lower than those induced by the addition of as-received RTS fibres (around 22% and 40% under the same replacement levels) (Wang *et al.* 2020). A similar finding was reported that utilising steel fibres with lower aspect ratios (72) to replace PE fibres with larger aspect ratios (765) improved the overall workability of EGC (Alrefaei and Dai 2018).

3.2 Drying shrinkage

The drying shrinkage of EGC can be induced by the evaporation of capillary water from the internal environment with a higher relative humidity to the external condition with a lower relative humidity (Yang *et al.* 2017). **Figure 6** depicts the effects of PVA and RTS fibre contents on the drying shrinkage of EGC, indicating that regardless of reinforcing fibre, the drying shrinkage of all mixtures evolved very rapidly at early ages and after which, the development rate was gradually reduced. The drying shrinkage of EGC with only PVA fibres became stable after about 10 d, while that of EGC containing hybrid PVA and RTS fibres flattened after 4 d. As the curing age increases, the internal microstructure of EGC is refined as a result of the continued chemical reactions, which intensifies the interaction between fibres and the matrix and therefore slows down the development of drying shrinkage. The deformed shape of RTS fibres can improve the bonding with the matrix by providing additional mechanical anchorage (Gong *et al.* 2022). Therefore, the drying shrinkage of EGC containing RTS fibres was considerably lower than that of PVA fibre reinforced EGC at various testing ages. For instance, the 28-d drying shrinkage of P1.75R0.25 and P1.5R0.5 was 58.37% and 65.61% respectively lower than that of P2. Previous studies also reported that the use of RTS fibres can lower the drying shrinkage of cementitious composites (Al-Musawi *et al.* 2019; Zhong and Zhang 2020). The higher strength and elastic modulus of RTS fibres also contributed to limiting the drying shrinkage of EGC. Combining PVA fibres with a suitable content of RTS fibres can create a synergistic effect to control the shrinkage-induced cracking, where short RTS fibres can effectively bridge the micro-cracks while PVA and long RTS fibres can control the macro-cracks. Increasing the PVA fibre dosage from 1.5% to 2.0% did not enhance the drying shrinkage of EGC, which can be attributed to the increased porosity (Zhong and Zhang 2021; Wang *et al.* 2022). It is worth noting that internal moisture can be lost more easily in

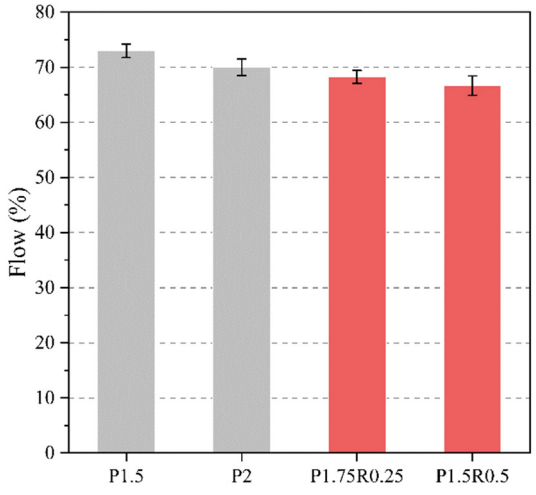

Fig. 5 Effects of PVA and RTS fibres on flowability of fresh EGC.

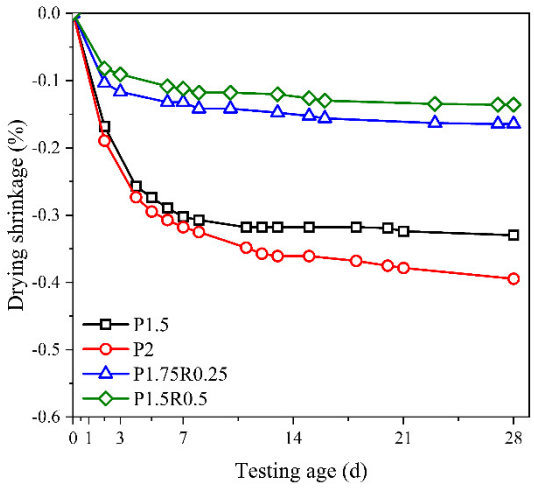

Fig. 6 Effects of PVA and RTS fibres on drying shrinkage of EGC.

Table 4 Uniaxial tensile properties of all mixtures.

Mix ID	Fist cracking strength (MPa)	Tensile strength (MPa)	Tensile strain capacity (%)	Strain energy density (kJm^{-3})	Average crack width (μm)
P1.5	1.83 (0.05)	4.37 (0.47)	5.15 (0.51)	161.93 (19.22)	111.35
P2	2.69 (0.11)	4.47 (0.27)	4.90 (0.23)	172.15 (11.77)	85.39
P1.75R0.25	2.58 (0.24)	4.70 (0.57)	4.92 (0.08)	163.38 (14.18)	78.72
P1.5R0.5	2.14 (0.16)	3.03 (0.01)	4.33 (0.24)	106.62 (3.93)	72.17

Note: The values in parentheses are standard deviations.

the presence of more pore networks, increasing the drying shrinkage (Afroughsabet and Teng 2020).

3.3 Uniaxial tensile behaviour

3.3.1 Tensile stress-strain response and failure pattern

The tensile stress-strain curves of all mixtures are presented in **Fig. 7**. For P1.75R0.25 and P1.5R0.5, only two curves were presented as the tensile failures of the third specimens did not occur within their gauge regions. Similar to other ECC and EGC specimens, the tensile stress-strain curves of all mixtures can be divided into two distinct parts, including a linear elastic region and a strain-hardening region. These curves were consistent with their failure patterns shown in **Fig. 8**, where multiple cracking features can be observed. The tensile stress-strain curves and failure patterns of P1.5, P2 and P1.75R0.25 were similar, while the strain-hardening region of P1.5R0.5 was the shortest along with the least number of cracks. The effect of RTS fibre on the uniaxial tensile performance of EGC will be further assessed by discussing the quantitative results in the next section.

3.3.2 Tensile properties

Table 4 summarizes the results of first cracking strength, tensile strength, tensile strain capacity, strain energy density and average crack width for all mixtures. It should be noted that the strain energy density is the strain energy per unit volume of EGC during the linear elastic and strain-hardening regions and was derived by integrating the tensile stress-strain curve up to the highest point of tensile stress (Xu *et al.* 2022; Yoo and Banthia 2022). A portable digital microscope was used to measure the crack width of EGC immediately after the tensile failure.

The first cracking strength of EGC went up with the increasing PVA fibre content but dropped as the RTS fibre replacement dosage increased. The first cracking strength of EGC is influenced by the matrix fracture toughness and internal pore structure as well as fibre bridging behaviour if the initial flaws are bridged by the fibres (Li 2019). P2 had the highest first cracking strength of 2.69 MPa, which can be ascribed to the stronger fibre bridging effect before the appearance of the first visible crack induced by the uniaxial tensile loading. A similar finding was also reported by previous studies (Ohno and Li 2018; Zhong and Zhang 2021) that the first cracking strengths of EGC with various PVA fibre contents were different when the same matrix component was employed.

Raising the PVA fibre dosage from 1.5% to 2.0% slightly improved the tensile strength of EGC while the tensile strain capacity dropped by 4.85%, consistent with that reported by Ohno and Li (2018) that the tensile strain capacity of EGC was reduced from 4.7% to 4.4% when the PVA fibre content changed from 1.5% to 2.0%. At the cracking plane, fibres aligning parallel to the loading direction with lower inclination angles can play a more effective bridging role. Some typical fibre orientations are illustrated in **Fig. 9(a)**. Fibre-1 and fibre-2 can better bridge the crack induced by the uniaxial tensile loading, while fibre-3 could not offer any restraining effect as its inclination angle is 90°. The in-situ strength of PVA fibres would be weakened when their inclination angles are

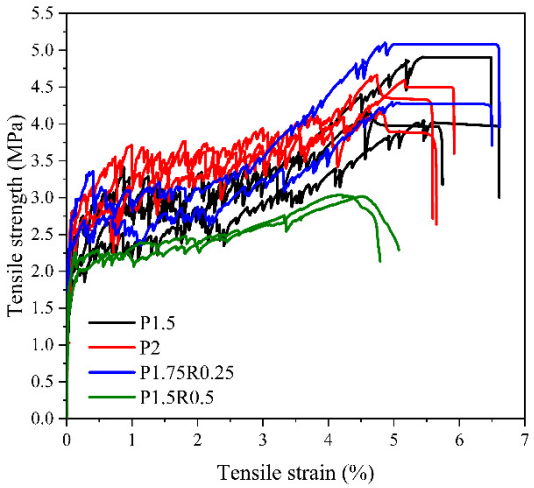

Fig. 7 Tensile stress-strain curves of all EGC mixtures.

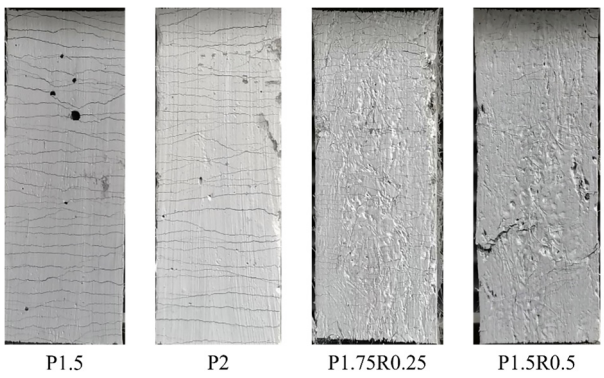

Fig. 8 Failure patterns of all EGC mixes after uniaxial tension.

too large (over 45°), rupturing more easily and thereby diminishing the overall bridging capacity (Li 2019; Li *et al.* 2021). In addition, the centroidal distance of the inclined fibres can also influence the overall fibre bridging capacity of the composites (Li 2019). As displayed in **Fig. 9(b)**, fibre-5 can still offer the bridging effect while fibre-4 is not counted as the bridging fibre at the cracking plane due to its large centroidal distance [$\geq \left(\frac{l_f}{2}\right)\cos(\theta)$], where l_f is the fibre length and θ is the inclination angle). These suggest that both fibre distribution and fibre orientation play a critical role in the uniaxial tensile behaviour of EGC. Nevertheless, the tensile performance of P2 was more stable than that of P1.5 given that the coefficient of variations of the tensile strength (6% against 11%) and tensile strain capacity (5% against 10%) were lower. Besides, the strain energy density of P2 was 6.3% greater than that of P1.5, indicating its better strain-hardening performance. The smaller residual crack width of P2, as compared with P1.5, revealed its stronger crack-controlling ability.

Replacing 0.25% PVA fibre with RTS fibre led to a 5.15% improvement in tensile strength and a comparable tensile strain capacity for EGC as compared to P2, which can be related mainly to the improved fibre-matrix bonding and high mechanical properties of RTS fibres. This can be supported by a previous study (Alrefaei and Dai 2018) that the tensile strength of fly ash-slag based EGC with 2.0% steel fibre was 10.84% better than that with 2.0% PE fibre due to the larger tensile strength of steel fibres against PE fibres. The unimproved tensile ductility can be linked to the reduced fibre bridging capacity as a result of the lower number of RTS fibres inside EGC compared to that of PVA fibres under the same incorporated fibre content. Due to the smaller diameter of PVA fibres, more PVA fibres can appear across a certain area within EGC, which increases the possibility of arising effective fibres at the crack interface and avoids the tensile failure localisation prior to the formation of a new crack, as illustrated in **Fig. 10(a)**. Thus, the tensile properties including tensile strength, tensile strain capacity and strain energy density were further weakened when more RTS fibres were employed to replace PVA fibres (P1.5R0.5). The crack widths of P1.75R0.25 and P1.5R0.5 were 7.81% and 15.48% smaller than that of P2, which can be attributed to the better RTS fibre-matrix interaction, as discussed above. The synergistic effect of RTS and PVA fibres in restraining the crack width of EGC can be observed in **Fig. 10(b)**, This agrees well with a previous study (Wang *et al.* 2020) that the average crack widths of EGC containing RTS fibres after four-point bending tests were 63 to 73% smaller than that of EGC incorporating 2.0% PVA fibre.

3.4 Quasi-static compressive strength

Figure 11 presents the effect of PVA and RTS fibre content on the quasi-static compressive strength of EGC. The compressive strength of P2 was 13.54% lower than that of P1.5 due to the lower compactness of the composite induced by the low elastic modulus of PVA fibres. More air voids can be introduced into the mixture after the addition of more PVA fibres, which would lead to a higher degree of compressibility (Ranjbar and Zhang 2020). By contrast, adding RTS fibres was beneficial to the quasi-

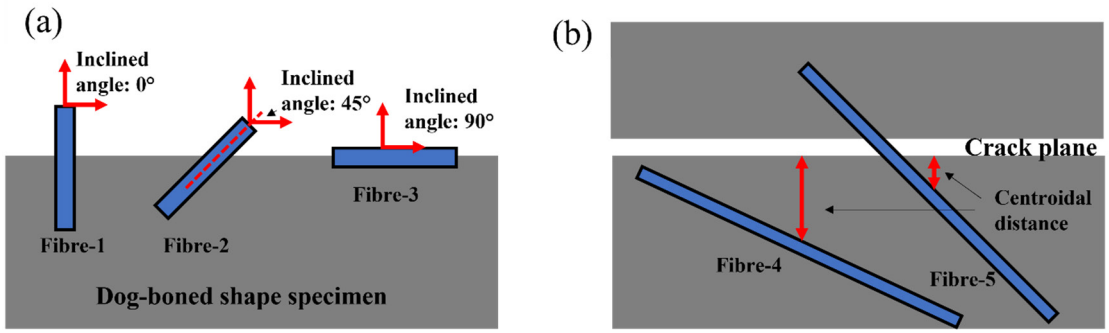

Fig. 9 Schematic illustration of fibre conditions at the cracking planes, based on (Li 2019; Ding *et al.* 2020).

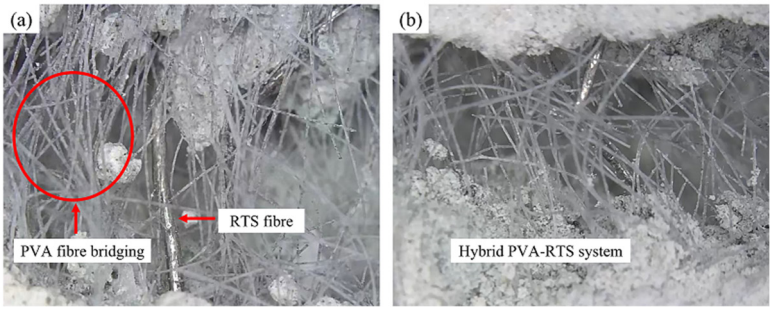

Fig. 10 Fibre status across the fracture surface of EGC.

static compressive strength of EGC. The compressive strengths of P1.75R0.25 and P1.5R0.5 were 8.04% and 30.72% higher than that of P2. This can be ascribed to the higher strength and elastic modulus of RTS fibres, better bonding between RTS fibres and the matrix, and synergistic effect of different fibres in restraining the cracks. The enhancement in compressive strength caused by the incorporation of 0.5% RTS fibre here was greater than that induced by the same volume fraction of unscreened RTS fibres (Wang *et al.* 2020). This is because the ununiform lengths and irregular shapes of as-received RTS fibres can lead to inconsistent performance in limiting the cracks. The ultimate compressive strength of EGC with RTS fibres could be weakened if RTS fibres are poorly distributed.

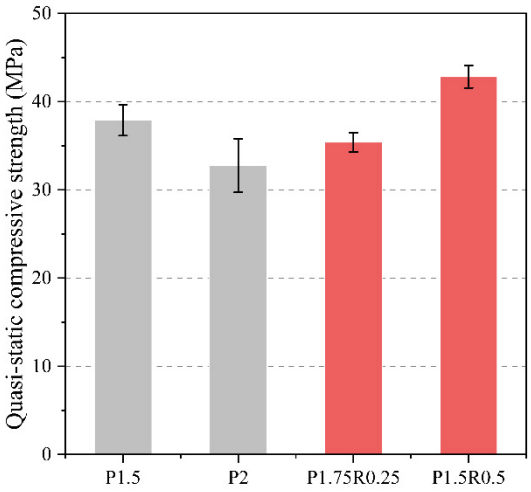

Fig. 11 Effects of PVA and RTS fibres on quasi-static compressive strength of EGC.

The typical compressive failure modes of all mixtures are illustrated in **Fig. 12**. No major difference can be observed for the failure patterns of all mixes. Unlike the brittle failure of plain geopolymers, all EGC mixtures maintained their integrity along with some visible cracks presenting on the surfaces.

3.5 Dynamic compressive behaviour

3.5.1 Failure pattern

The dynamic compressive failure patterns of all mixtures under various strain rates are demonstrated in **Fig. 13**, indicating that the damage degree of all specimens was sensitive to strain rate. The resulted strain rates caused by impact velocities of 6 ms^{-1}, 8 ms^{-1} and 10 ms^{-1} were in ranges of 40 to 60 s^{-1}, 80 to 130 s^{-1} and 130 to 180 s^{-1}, respectively. The failure modes can be distinguished into three types including slight edge cracking failure, splitting cracking failure and fragmentation failure. When the strain rate was below 126.6 s^{-1}, all EGC specimens can still maintain intact while after which, all mixes were disintegrated into several irregular broken fragments. At a lower strain rate, the impact energy was consumed by the

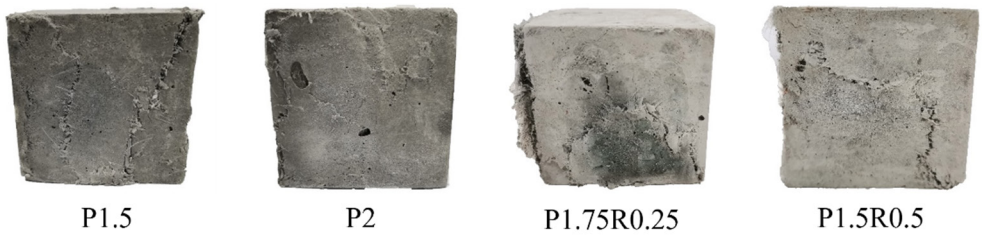

Fig. 12 Failure modes of EGC mixtures after quasi-static compression.

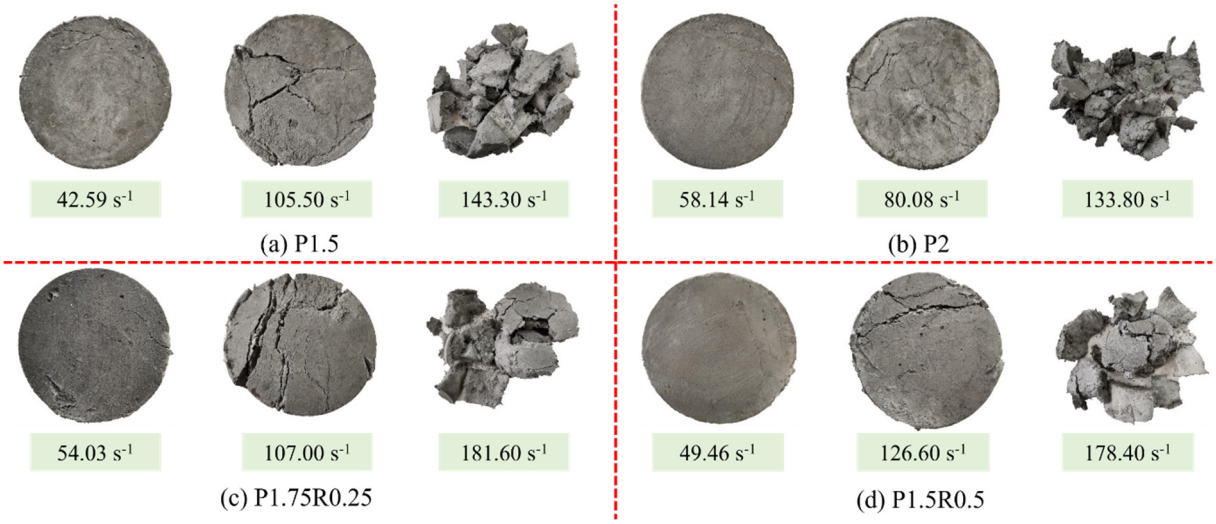

Fig. 13 Typical dynamic compressive failure patterns of all EGC mixtures.

crack propagation from the edge of the test specimen towards its core area. Meanwhile, the fibre bridging behaviour can significantly restrain the generated cracks, retaining the shape of the sample. As the strain rate rises, the impact energy and crack velocity go up simultaneously, generating more cracks to consume the energy before the crack development (Yu *et al.* 2021). The fibre bridging efficiency would be weakened due to the larger crack size and most fibres were either pulled out (completely or partly) or ruptured. Only a few fibres can bridge the broken pieces.

Changing the PVA fibre content did not lead to obvious changes in the failure patterns of EGC at various strain rates. As indicated in a previous study (Xiao *et al.* 2021), the damage degree of fly ash-slag based geopolymer composites with 1.2% PVA fibre was more serious than that containing 0.6% PVA fibre, while a different conclusion was reported in another study (Zhong and Zhang 2022b) that increasing the PVA fibre content from 1.0% to 2.0% reduced the dynamic compressive damage level of EGC. Like static mechanical properties, fibre distribution and fibre orientation can affect the dynamic failure pattern of EGC substantially, where fibres aligned perpendicular to the loading direction would be more effective in restraining the cracks caused by the dynamic compression. The failure patterns of EGC containing RTS fibres were similar to that of P2 when the strain rate was lower than 126.6 s^{-1}. At a higher strain rate, the presence of RTS fibres mitigated the damage of test specimens, where the fragment sizes were larger compared to that of P2, which can be associated with the stronger bridging effect of RTS fibres when facing a larger size of the crack and the crack-controlling synergy created by hybrid PVA and RTS fibres. Additionally, the bridging capacity of PVA fibres could be weakened at a high strain rate due to their extraordinary interface bonding with the matrix (Boshoff *et al.* 2009; Yang and Li 2014; Curosu *et al.* 2016; Farooq *et al.* 2022), which may lower the resistance of EGC to dynamic compressive cracking.

3.5.2 Stress-strain response

Figure 14 depicts the dynamic compressive stress-strain curves of all mixes under various strain rates. Under dynamic compression, EGC specimens experienced elastic deformations in the initial stage and after reaching the elastic limit, the cracks inside the samples were initiated and propagated with the rising strain, which cause a non-

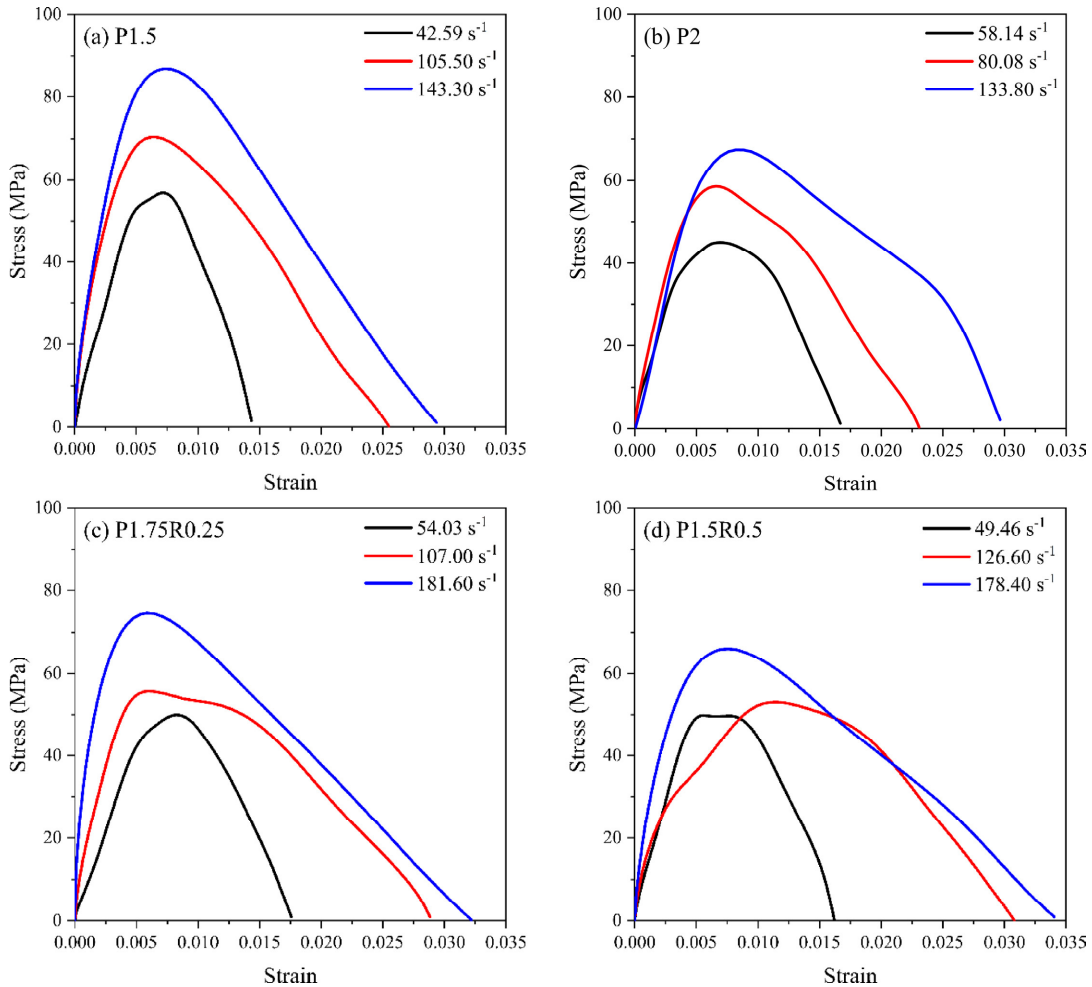

Fig. 14 Dynamic compressive stress-strain curves of (a) P1.5, (b) P2, (c) P1.75R0.25, and (d) P1.5R0.5.

linear stress-strain behaviour. The strain increment rate can be limited by the bridging fibres. When exceeding the peak stress, the induced cracks would be further propagated and expanded. The bridging fibres crossing these cracks were either pulled out or ruptured during the sliding/slippage process. As discussed in Section 3.5.1, the crack velocity tends to be higher at a larger strain rate. This can be evidenced here that the slope of the curve up to the peak stress went up with the strain rate, corresponding to faster rates of crack initiation and development. Similar to other fibre reinforced geopolymer composites (Khan *et al.* 2018; Xiao *et al.* 2021) and mono-PVA fibre reinforced EGC (Zhong and Zhang 2022b), the dynamic compressive strength (peak stress) of all mixtures was strain-rate dependent. For instance, the dynamic compressive strength of P1.75R0.25 was improved by 11.49% and 49.42% when the strain rate changed from 54.03% to 107 s^{-1} and 181.6 s^{-1}, respectively. This can be ascribed mainly to the Stefan effect, cracking propagation effect and some structural effects (Lai and Sun 2009; Hao *et al.* 2013; Ren *et al.* 2015). The structural factors including lateral inertia and end friction effects may not be the dominant reasons here because of the selected specimen size, considered test strain rate range, and the use of grease before the test (Bertholf and Karnes 1975; Zhang *et al.* 2009; Khan *et al.* 2018). The peak strain (strain at the peak stress) of EGC was mostly greater at a higher strain rate as the increasing number of cracks can result in a larger specimen deformation.

3.5.3 Dynamic compressive strength

Figure 15 presents the dynamic compressive strength and energy absorption capacity of EGC under different strain rates. Like quasi-static compressive strength, the dynamic compressive strength of P2 was lower than that of P1.5 at all test strain rates. As mentioned earlier, the weakened workability could lead to poor fibre dispersion and high porosity for P2, limiting the fibre bridging behaviour and the generation of new cracks. The poor fibre dispersion would not be favourable for inducing the effective fibre orientation and thereby, the overall fibre bridging capacity would be impaired. P1.5 with better fibre distribution and orientation can effectively reduce the dynamic deformation of EGC, improving the dynamic compressive strength. As seen in **Figs. 14(a)** and **14(b)**, the peak strain of P1.5 was smaller than that of P2 within the strain rate range of 80.08 to 143.3 s^{-1}. The properties and interfacial bonding properties of PVA fibres were reported to be sensitive to the strain rate as well, where around 55% and 64% increments in tensile and bond strengths were observed for PVA fibres when the loading rate increased from 0.005 mms^{-1} to 50 mms^{-1} (Curosu *et al.* 2016). These would induce more pulled out PVA fibres, which absorb more energy and therefore enhance the dynamic compressive strength. Nevertheless, the probability of fibre rupture in ECC was found to go up with the rising loading rate (Boshoff *et al.* 2009) and the chemical bonding of ECC with PVA fibres at the testing speed of 10 mms^{-1} was approximately 5 times higher than that at 10^{-3} mms^{-1}. The superior chemical bonding could result in fibre rupture before the pull-out process, impairing the fibre bridging effect considerably. Hence, the dynamic compressive strength of EGC was not enhanced with the increase of PVA fibre dosage.

Owing to the insignificant strain rate sensitivity of steel fibres (Su *et al.* 2016; Nieuwoudt and Boshoff 2017), the presence of RTS fibres in EGC can compensate for the loss of bridging capacity caused by ruptured PVA fibres, especially at a larger strain rate. Although RTS fibres are also hydrophilic, the appropriate fibre-matrix bonding along with the additional anchorage is conducive to inducing fibre pull-out instead of fibre rupture, bridging the cracks effectively. When the strain rate was between 133.8 s^{-1} and 181.6 s^{-1}, the dynamic compressive strength of P1.75R0.25 was 10.63% higher than that of P2. However, P1.5 still outperformed hybrid PVA-RTS fibre reinforced EGC because of its better internal structure with lower porosity and superior fibre dispersion.

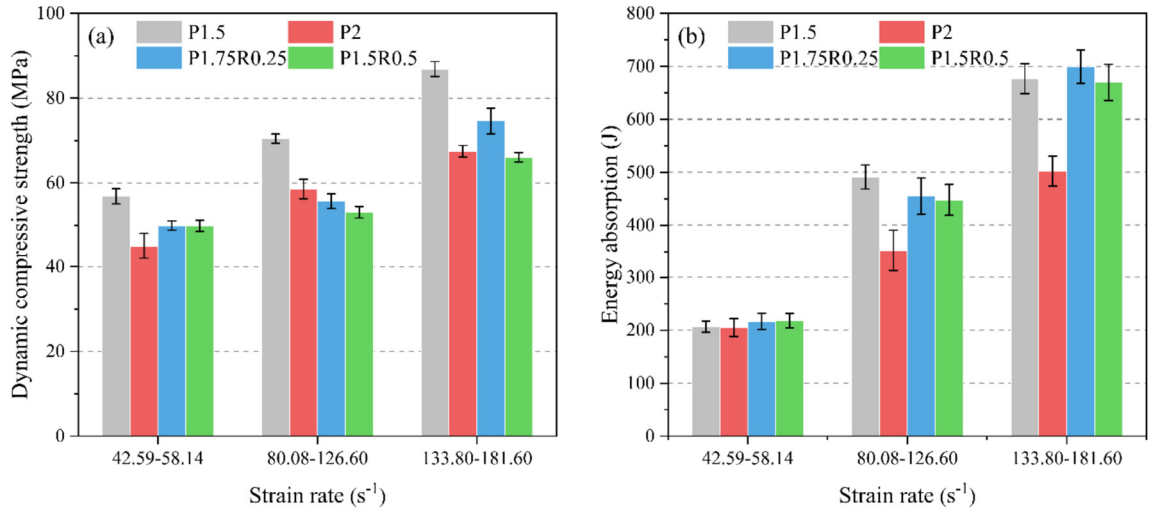

Fig. 15 Effects of strain rate and fibre on (a) dynamic compressive strength, and (b) energy absorption capacity of EGC.

As seen in **Fig. 15(b)**, the changing tendency of energy absorption capacity with the strain rate was similar to that of dynamic compressive strength. For plain concrete, its energy absorption only comes from the generation and propagation of cracks while for EGC, additional energy is needed to pull out or rupture the incorporated fibres to finally fracture the whole composites. At the strain rate of 42.59 to 58.14 s^{-1}, the energy absorption capacity of all mixtures was comparable, and the calculated energy absorption could be underestimated as the specimens within this strain rate range were not completely fractured (see **Fig. 13**) (Khan *et al.* 2018). At higher strain rates, raising the PVA fibre content was still not beneficial to the energy absorption capacity of EGC. By contrast, replacing PVA fibres with RTS fibres improved the energy absorption capacity of EGC considerably. For instance, the absorbed energy of P1.75R0.25 and P1.5R0.5 was about 29 to 39% and 27 to 33% respectively greater than that of P2 when the strain rate was within 80.08 s^{-1} and 181.6 s^{-1}. This was primarily related to the reduced number of ruptured PVA fibres. It is worth noting that the energy absorption capacity of P1.75R0.25 was even better than P1.5 at the strain rate of 133.8 to 181.6 s^{-1}.

DIF was calculated by dividing the dynamic compressive strength by the quasi-static compressive strength, the results of which are demonstrated in **Fig. 16(a)**. The changing tendency of DIF with the strain rate and fibre was similar to that of dynamic compressive strength. The increase rate of DIF for mono-PVA fibre reinforced EGC (24 to 53%) was greater than that for hybrid PVA-RTS fibre reinforced EGC (6 to 49%), which can be mainly associated with the lower strain rate sensitivity of steel fibres as compared with PVA fibres. The DIF results here were also used to compare with the existing DIF models for normal concrete, as displayed in **Fig. 16(b)**. The *fib* Model Code for Concrete Structures (*fib* 2013) and CEB-FIP Model Code 1990 (CEB-FIP 1993) are two reliable models to predict the DIF of normal-strength concrete, as described below:

$$\begin{cases} DIF_{FIB} = \left(\dfrac{\dot{\varepsilon}}{\dot{\varepsilon}_1}\right)^{0.014}, & \text{for } \dot{\varepsilon} \le 30s^{-1} \\ DIF_{FIB} = 0.012\left(\dfrac{\dot{\varepsilon}}{\dot{\varepsilon}_1}\right)^{\frac{1}{3}}, & \text{for } \dot{\varepsilon} > 30s^{-1} \end{cases} \tag{4}$$

$$\begin{cases} DIF_{CEB-FIP} = \left(\dfrac{\dot{\varepsilon}}{\dot{\varepsilon}_1}\right)^{1.026\alpha}, & \text{for } \dot{\varepsilon} \le 30s^{-1} \\ DIF_{CEB-FIP} = \gamma\left(\dfrac{\dot{\varepsilon}}{\dot{\varepsilon}_1}\right)^{\frac{1}{3}}, & \text{for } \dot{\varepsilon} > 30s^{-1} \end{cases} \tag{5}$$

where $\dot{\varepsilon}_1 = 0.00003s^{-1}$, $\alpha = \dfrac{1}{\left(5+9\dfrac{f_c}{f_{c1}}\right)}$, $\gamma = 10^{(6.156\alpha-2)}$, f_c stands for the quasi-static compressive strength, and $f_{c1} = 10$ MPa.

$30s^{-1}$ is considered as the transition strain rate and over which, the DIF rises dramatically with the increasing strain rate. As the strain rate went up, the DIF results of mono-PVA fibre reinforced EGC approached the CEB-FIP model while those of EGC with hybrid fibres deviated significantly from both *fib* and CEB-FIP models. The transition strain rates for hybrid fibre reinforced EGC were greater than those for mono-fibre reinforced EGC. In comparison with the DIF results obtained from the existing literature (Khan *et al.* 2018; Xiao *et al.* 2021; Zhong and Zhang 2022b), the DIF values here were comparable at a strain rate of lower than 100 s^{-1} but those of EGC containing RTS fibres were smaller when the strain rate was higher than 100 s^{-1}. In addition, the DIF of hybrid steel-PE fibre reinforced geopolymer composites

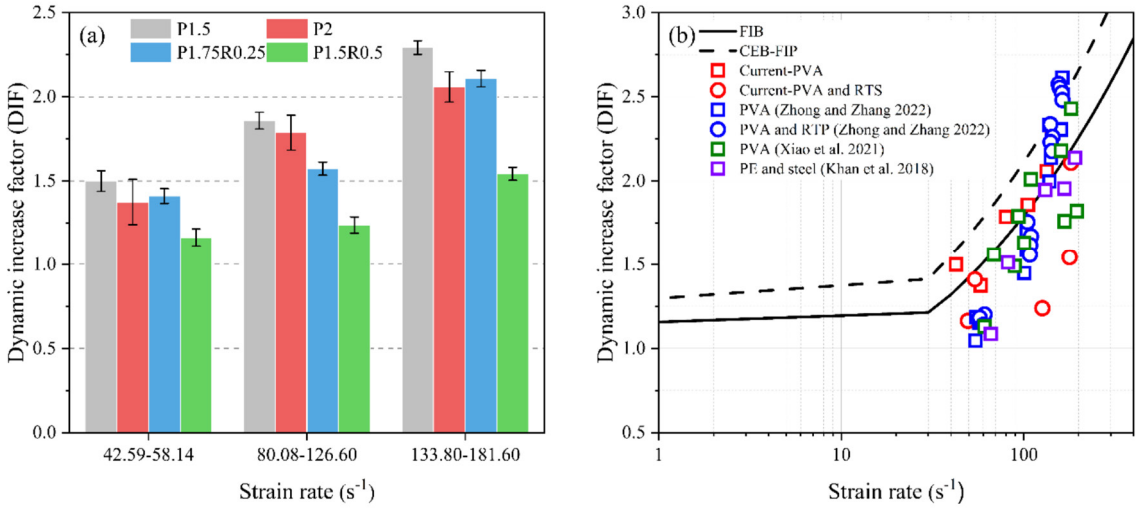

Fig. 16 DIF of all EGC mixtures: (a) effects of strain rate and fibre, and (b) comparison with predictions by existing models and literature (CEB-FIP 1993; *fib* 2013; Khan *et al.* 2018; Xiao *et al.* 2021; Zhong and Zhang 2022b).

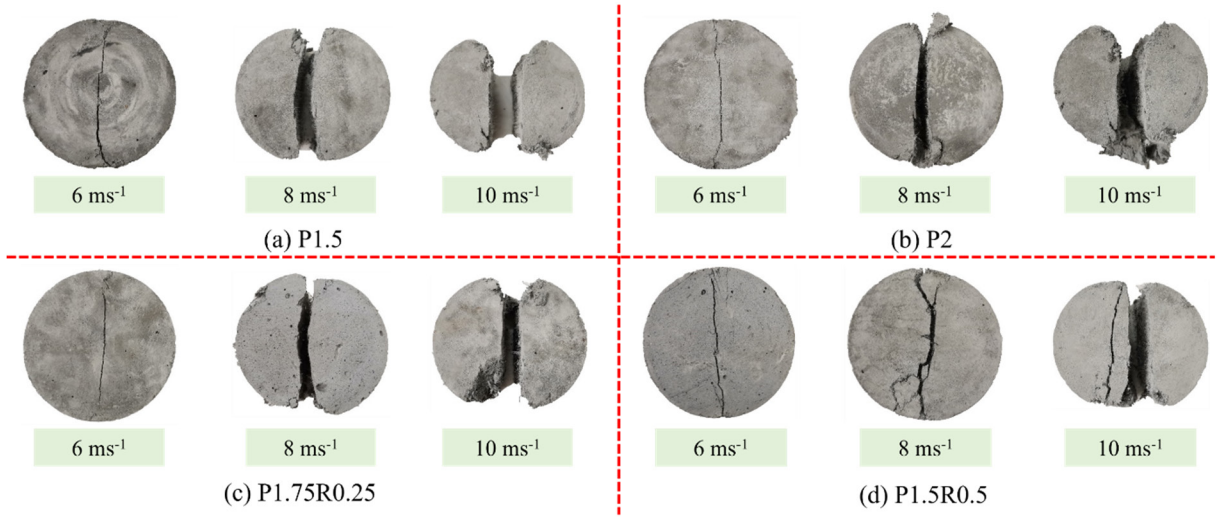

Fig. 17 Typical dynamic splitting failure patterns of all EGC mixtures.

was generally lower than that of mono-PVA fibre reinforced EGC, consistent with our previous discussion. The discrepancies observed here can be ascribed to the different macroscopic properties and microstructure between disparate mixes.

3.6 Dynamic splitting tensile behaviour

3.6.1 Failure pattern

Figure 17 displays the typical failure modes of EGC after dynamic splitting tension, indicating that all tests were valid as the major cracks passed through the central portions of test specimens. Like the strain rate effect on the dynamic compressive failure mode of EGC, increasing the impact velocity intensified the damage on the sample along with a larger crack width. At the impact velocity of 6 ms^{-1}, the major splitting cracks were still connected by the bridging fibres while most mixtures disintegrated into two parts when the impact velocity reached 8 ms^{-1}. Under this impact velocity, only P1.5R0.5 was not split into two parts and many derivative cracks can be observed along the major crack, implying its superior ductility. The strong bridging effect of RTS fibres can disperse the splitting stress to the surrounding areas, generating additional cracks. At the highest impact velocity (10 ms^{-1}), all mixtures presented pronounced triangular damage near the loading ends, which can be induced by the increased stress concentration near the two ends. Similar phenomena were also captured in previous studies (Khan *et al.* 2019; Zhong and Zhang 2022a) and increasing the fibre dosage did not effectively mitigate such damage. Some studies pre-treated the loading surfaces of the test sample before the dynamic splitting tension while the triangular damage failure can still be observed (Feng *et al.* 2018; Chen *et al.* 2020). However, the triangular damage near two loading ends was lessened when 0.5% PVA fibre was replaced with RTS fibre [see **Fig. 17(d)**].

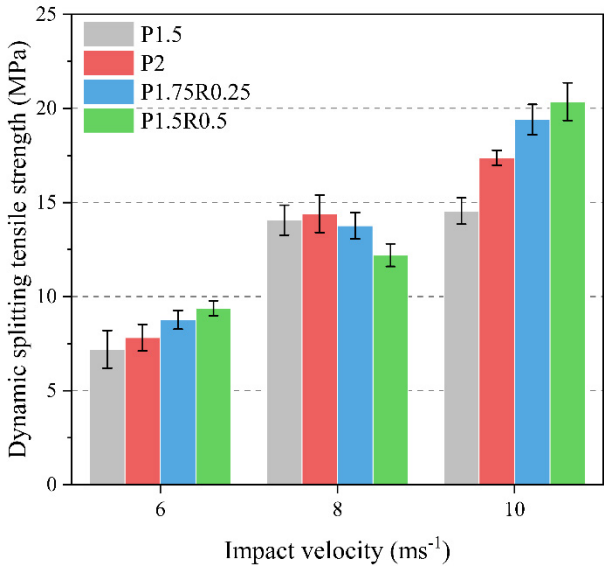

Fig. 18 Effects of impact velocity and fibre on dynamic splitting tensile strength of EGC.

3.6.2 Dynamic splitting tensile strength

Figure 18 illustrates the effects of impact velocity and fibre content on the dynamic splitting tensile strength of EGC. The dynamic splitting tensile strength of all mixtures exhibited a strong sensitivity to the impact velocity and the causing reasons are similar to those explained for dynamic compressive strength. Different from dynamic compression, only one major crack was induced by the dynamic splitting tension and the effective fibre bridging action across the cracking interface can substantially enhance the ultimate strength of EGC. In addition, the dynamic splitting tensile strength of P2 was 2.38 to 19.43% greater than that of P1.5 under various impact velocities due to the presence of more PVA fibres along the major cracks. Under dynamic compression, the fibre distribution and orientation inside the whole specimen are essential as cracks are generated randomly and simultaneously while for dynamic splitting tension, only the fibres near the major crack can play a critical role. At the impact velocity of 6 ms^{-1} and 10 ms^{-1}, the dynamic splitting strengths of P1.75R0.25 and P1.5R0.5 were 11.72 to

12.12% and 17.21 to 20.04% higher than that of P2, respectively, which can be attributed mainly to those mentioned previously in Section 3.5.3. However, an opposite trend can be identified at the impact velocity of 8 ms^{-1} that increasing the RTS fibre content led to a reduced dynamic splitting tensile strength for EGC. This could be related to the inconsistent behaviour of each RTS fibre as some fibres could be damaged during the recycling process, resulting in an unstable performance for the resultant composites (Skarżyński and Suchorzewski 2018; Zhong and Zhang 2020). Future studies are required to explore the effect of more impact velocities on the dynamic splitting tensile behaviour of EGC to better understand the inconsistency observed in this study.

4. Conclusions

This paper presents a systematic experimental study on the effects of polyvinyl alcohol (PVA) and recycled tyre steel (RTS) fibres on the static and dynamic mechanical properties of ambient-cured fly ash-slag based engineered geopolymer composites (EGC). Based on the results obtained, the main conclusions can be drawn as follows:

(1) The workability of EGC was slightly weakened with the increasing PVA and RTS fibre dosages. Raising the PVA fibre content from 1.5% to 2.0% impaired the drying shrinkage resistance of EGC due to the increased porosity, while the 28-d drying shrinkage of EGC with 0.25% RTS fibre and 0.5% RTS fibre was 58.37% and 65.61% respectively lower than that of EGC containing 2.0% PVA fibre.

(2) All EGC mixes existed obvious strain-hardening and multiple cracking features. The uniaxial tensile properties of EGC were not significantly improved by increasing the PVA fibre content. Replacing 0.25% PVA fibre with RTS fibre slightly enhanced the tensile strength of EGC but further incorporation of RTS fibre to 0.5% weakened the tensile properties of EGC. The quasi-static compressive strength of EGC went up by 31% when 0.5% PVA fibre was replaced with RTS fibre.

(3) Regardless of reinforcing fibre type, the dynamic compressive properties including dynamic compressive strength, peak strain, dynamic increase factor and energy absorption capacity of EGC were strongly sensitive to strain rate. EGC with 1.5% PVA fibre outperformed EGC containing 2.0% PVA fibre because of the better microstructure and superior fibre distribution. The insignificant strain rate sensitivity of RTS fibres and their higher mechanical properties compared to PVA fibres contributed to enhancing the dynamic compressive properties and reducing the damage of EGC.

(4) The dynamic splitting tensile strength of EGC can be improved by rising the PVA fibre dosage or substituting PVA fibres with RTS fibres. The dynamic splitting tensile strength of EGC with hybrid PVA and RTS fibres was about 12 to 20% greater than that of mono-PVA fibre reinforced EGC.

(5) This study reveals that employing 0.25 to 0.5% RTS fibre to replace PVA fibre can improve the drying shrinkage resistance and static and dynamic compressive properties of EGC while maintaining acceptable uniaxial tensile behaviour. Towards practical applications of such sustainable composites, the effect of RTS fibre on durability under different loading conditions needs to be explored.

Acknowledgements

The authors gratefully acknowledge the financial support from the Engineering and Physical Sciences Research Council (EPSRC) under Grant No. EP/R041504/1 and the Royal Society under Award No. IEC/NSFC/191417. The financial support provided by University College London (UCL) and China Scholarship Council (CSC) to the first author is gratefully acknowledged.

References

Afroughsabet, V. and Teng, S., (2020). "Experiments on drying shrinkage and creep of high performance hybrid-fiber-reinforced concrete." *Cement and Concrete Composites*, 106, 103481.

Al-Musawi, H., Figueiredo, F. P., Guadagnini, M. and Pilakoutas, K., (2019). "Shrinkage properties of plain and recycled steel-fibre-reinforced rapid hardening mortars for repairs." *Construction and Building Materials*, 197, 369-384.

Alrefaei, Y. and Dai, J.-G., (2018). "Tensile behavior and microstructure of hybrid fiber ambient cured one-part engineered geopolymer composites." *Construction and Building Materials*, 184, 419-431.

ASTM, (2015). "*Standard test method for flow of hydraulic cement mortar* (ASTM C1437-15)." West Conshohocken, PA, USA: ASTM International.

ASTM, (2017a). "*Standard practice for use of apparatus for the determination of length change of hardened cement paste, mortar, and concrete* (ASTM C490-17)." West Conshohocken, PA, USA: ASTM International.

ASTM, (2017b). "*Standard specification for coal fly ash and raw or calcined natural pozzolan for use in concrete* (ASTM C618-17a)." West Conshohocken, PA, USA: ASTM International.

ASTM, (2020). "*Standard test method for compressive strength of hydraulic cement mortars using 2-in. or 50-mm cube specimens* (ASTM C109/C109M-20b)." West Conshohocken, PA, USA: ASTM International.

Bertholf, L. D. and Karnes, C. H., (1975). "Two-dimensional analysis of the split Hopkinson pressure bar system." *Journal of the Mechanics and Physics of Solids*, 23(1), 1-19.

Boshoff, W. P., Mechtcherine, V. and van Zijl, G. P. A. G., (2009). "Characterising the time-dependant behaviour on the single fibre level of SHCC: Part 2: The rate effects on fibre pull-out tests." *Cement and Concrete Research*, 39(9), 787-797.

CEB-FIP, (1993). "*CEB-FIP model code 1990: Design code* (CEB Bulletin d'Information No 213/214)." Lausanne, Switzerland: Comité Euro International du Béton.

Chen, M., Chen, W., Zhong, H., Chi, D., Wang, Y. and Zhang, M., (2019). "Experimental study on dynamic compressive behaviour of recycled tyre polymer fibre reinforced concrete." *Cement and Concrete Composites*, 98, 95-112.

Chen, M., Zhong, H., Wang, H. and Zhang, M., (2020). "Behaviour of recycled tyre polymer fibre reinforced concrete under dynamic splitting tension." *Cement and Concrete Composites*, 114, 103764.

Chen, W. and Song, B., (2011). "*Split Hopkinson (Kolsky) bar: Design, testing and applications*." New York: Springer-Verlag New York Inc.

Choi, W.-C., Yun, H.-D., Kang, J.-W. and Kim, S.-W., (2012). "Development of recycled strain-hardening cement-based composite (SHCC) for sustainable infrastructures." *Composites Part B: Engineering*, 43(2), 627-635.

Curosu, I., Mechtcherine, V. and Millon, O., (2016). "Effect of fiber properties and matrix composition on the tensile behavior of strain-hardening cement-based composites (SHCCs) subject to impact loading." *Cement and Concrete Research*, 82, 23-35.

Ding, C., Guo, L. and Chen, B., (2020). "Orientation distribution of polyvinyl alcohol fibers and its influence on bridging capacity and mechanical performances for high ductility cementitious composites." *Construction and Building Materials*, 247, 118491.

Farooq, M., Krishna, A. and Banthia, N., (2022). "Highly ductile fiber reinforced geopolymers under tensile impact." *Cement and Concrete Composites*, 126, 104374.

Feng, W., Liu, F., Yang, F., Li, L. and Jing, L., (2018). "Experimental study on dynamic split tensile properties of rubber concrete." *Construction and Building Materials*, 165, 675-687.

fib, (2013). "*Model code for concrete structures 2010*." Lausanne, Switzerland: Fédération Internationale du Béton.

Gong, J., Ma, Y., Fu, J., Hu, J., Ouyang, X., Zhang, Z. and Wang, H., (2022). "Utilization of fibers in ultra-high performance concrete: A review." *Composites Part B: Engineering*, 241, 109995.

Hao, Y., Hao, H., Jiang, G. P. and Zhou, Y., (2013). "Experimental confirmation of some factors influencing dynamic concrete compressive strengths in high-speed impact tests." *Cement and Concrete Research*, 52, 63-70.

Isa, M. N., Pilakoutas, K., Guadagnini, M. and Angelakopoulos, H., (2020). "Mechanical performance of affordable and eco-efficient ultra-high performance concrete (UHPC) containing recycled tyre steel fibres." *Construction and Building Materials*, 255, 119272.

JSCE, (2008). "*Recommendations for design and construction of high performance fiber reinforced cement composites with multiple fine cracks (HPFRCC)*." Tokyo: Japan Society of Civil Engineers.

Khan, M. Z. N., Hao, Y., Hao, H. and Shaikh, F. U. A., (2018). "Experimental evaluation of quasi-static and dynamic compressive properties of ambient-cured high-strength plain and fiber reinforced geopolymer composites." *Construction and Building Materials*, 166, 482-499.

Khan, M. Z. N., Hao, Y., Hao, H. and Shaikh, F. U. A., (2019). "Mechanical properties and behaviour of high-strength plain and hybrid-fiber reinforced geopolymer composites under dynamic splitting tension." *Cement and Concrete Composites*, 104, 103343.

Lai, D., Demartino, C. and Xiao, Y., (2022). "High-strain rate tension behavior of fiber-reinforced rubberized concrete." *Cement and Concrete Composites*, 131, 104554.

Lai, J. and Sun, W., (2009). "Dynamic behaviour and visco-elastic damage model of ultra-high performance cementitious composite." *Cement and Concrete Research*, 39(11), 1044-1051.

Lao, J.-C., Xu, L.-Y., Huang, B.-T., Dai, J.-G. and Shah, S. P., (2022). "Strain-hardening ultra-high-performance geopolymer concrete (UHPGC): Matrix design and effect of steel fibers." *Composites Communications*, 30, 101081.

Li, J., Weng, J., Chen, Z. and Yang, E.-H., (2021). "A generic model to determine crack spacing of short and randomly oriented polymeric fiber-reinforced strain-hardening cementitious composites (SHCC)." *Cement and Concrete Composites*, 118, 103919.

Li, V. C., (2008). "Engineered cementitious composites (ECC): Material, structural, and durability performance." In: E. G. Nawy, Ed. *Concrete Construction Engineering Handbook*. Boca Raton, FL, USA: CRC Press, Chapter 24.

Li, V. C., (2019). "*Engineered cementitious composites (ECC): Bendable concrete for sustainable and resilient infrastructure*." Berlin: Springer-Verlag GmbH Germany.

Liew, K. M. and Akbar, A., (2020). "The recent progress of recycled steel fiber reinforced concrete." *Construction and Building Materials*, 232, 117232.

Lu, C., Yu, J. and Leung, C. K. Y., (2018). "Tensile performance and impact resistance of strain hardening cementitious composites (SHCC) with recycled fibers." *Construction and Building Materials*, 171, 566-576.

Luukkonen, T., Abdollahnejad, Z., Yliniemi, J., Kinnunen, P. and Illikainen, M., (2018). "One-part alkali-activated materials: A review." *Cement and Concrete Research*, 103, 21-34.

Merli, R., Preziosi, M., Acampora, A., Lucchetti, M. C. and Petrucci, E., (2019). "Recycled fibers in reinforced concrete: A systematic literature review." *Journal of Cleaner Production*, 248, 119207.

Nematollahi, B., Sanjayan, J., Qiu, J. and Yang, E.-H., (2017a). "High ductile behavior of a polyethylene

fiber-reinforced one-part geopolymer composite: A micromechanics-based investigation." *Archives of Civil and Mechanical Engineering*, 17(3), 555-563.

Nematollahi, B., Sanjayan, J., Qiu, J. and Yang, E.-H., (2017b). "Micromechanics-based investigation of a sustainable ambient temperature cured one-part strain hardening geopolymer composite." *Construction and Building Materials*, 131, 552-563.

Nieuwoudt, P. D. and Boshoff, W. P., (2017). "Time-dependent pull-out behaviour of hooked-end steel fibres in concrete." *Cement and Concrete Composites*, 79, 133-147.

Ohno, M. and Li, V. C., (2018). "An integrated design method of engineered geopolymer composite." *Cement and Concrete Composites*, 88, 73-85.

Paulay, T. and Binney, J. R., (1974). "Diagonally reinforced coupling beams of shear walls." *ACI Symposium Publication*, 42(2), 579-598.

Provis, J. L. and Van Deventer, J. S. J., (2009). "*Geopolymers: Structures, processing, properties and industrial applications*." Cambridge, UK: Woodehead Publishing.

Ranjbar, N. and Zhang, M., (2020). "Fiber-reinforced geopolymer composites: A review." *Cement and Concrete Composites*, 107, 103498.

Ren, W., Xu, J., Liu, J. and Su, H., (2015). "Dynamic mechanical properties of geopolymer concrete after water immersion." *Ceramics International*, 41(9-B), 11852-11860.

Rokugo, K. and Kanda, K., (2013). "*Strain hardening cement composites: Structural design and performance* (State-of-the-art report of the RILEM technical committee 208-HFC-SC3)." Dordrecht, The Netherlands: Springer Netherlands.

Rokugo, K., Kanda, T., Yokota, H. and Sakata, N., (2009). "Applications and recommendations of high performance fiber reinforced cement composites with multiple fine cracking (HPFRCC) in Japan." *Materials and Structures*, 42(9), 1197-1208.

Skarżyński, Ł. and Suchorzewski, J., (2018). "Mechanical and fracture properties of concrete reinforced with recycled and industrial steel fibers using digital image correlation technique and x-ray micro computed tomography." *Construction and Building Materials*, 183, 283-299.

Su, Y., Li, J., Wu, C., Wu, P. and Li, Z.-X., (2016). "Influences of nano-particles on dynamic strength of ultra-high performance concrete." *Composites Part B: Engineering*, 91, 595-609.

Wang, S. and Li, V. C., (2007). "Engineered cementitious composites with high-volume fly ash." *ACI Materilas Journal*, 104(3), 233-241.

Wang, Y., Chan, C. L., Leong, S. H. and Zhang, M., (2020). "Engineering properties of strain hardening geopolymer composites with hybrid polyvinyl alcohol and recycled steel fibres." *Construction and Building Materials*, 261, 120585.

Wang, Y., Zhong, H. and Zhang, M., (2022). "Experimental study on static and dynamic properties of fly ash-slag based strain hardening geopolymer composites." *Cement and Concrete Composites*, 129, 104481.

Xiao, S.-H., Liao, S.-J., Zhong, G.-Q., Guo, Y.-C., Lin, J.-X., Xie, Z.-H. and Song, Y., (2021). "Dynamic properties of PVA short fiber reinforced low-calcium fly ash-slag geopolymer under an SHPB impact load." *Journal of Building Engineering*, 44, 103220.

Xu, L.-Y., Huang, B.-T., Lan-Ping, Q. and Dai, J.-G., (2022). "Enhancing long-term tensile performance of engineered cementitious composites (ECC) using sustainable artificial geopolymer aggregates." *Cement and Concrete Composites*, 133, 104676.

Yang, E.-H. and Li, V. C., (2014). "Strain-rate effects on the tensile behavior of strain-hardening cementitious composites." *Construction and Building Materials*, 52, 96-104.

Yang, T., Zhu, H. and Zhang, Z., (2017). "Influence of fly ash on the pore structure and shrinkage characteristics of metakaolin-based geopolymer pastes and mortars." *Construction and Building Materials*, 153, 284-293.

Yoo, D.-Y. and Banthia, N., (2022). "High-performance strain-hardening cementitious composites with tensile strain capacity exceeding 4%: A review." *Cement and Concrete Composites*, 125, 104325.

Yu, J. and Leung, C. K., (2017). "Strength improvement of strain-hardening cementitious composites with ultrahigh-volume fly ash." *Journal of Materials in Civil Engineering*, 29, 05017003.

Yu, J., Yao, J., Lin, X., Li, H., Lam, J. Y. K., Leung, C. K. Y., Sham, I. M. L. and Shih, K., (2018). "Tensile performance of sustainable strain-hardening cementitious composites with hybrid PVA and recycled PET fibers." *Cement and Concrete Research*, 107, 110-123.

Yu, Q., Zhuang, W. and Shi, C., (2021). "Research progress on the dynamic compressive properties of ultra-high performance concrete under high strain rates." *Cement and Concrete Composites*, 124, 104258.

Yu, R., Spiesz, P. and Brouwers, H. J. H., (2014). "Static properties and impact resistance of a green ultra-high performance hybrid fibre reinforced concrete (UHPHFRC): Experiments and modeling." *Construction and Building Materials*, 68, 158-171.

Zhang, D., Yu, J., Wu, H., Jaworska, B., Ellis, B. R. and Li, V. C., (2020a). "Discontinuous micro-fibers as intrinsic reinforcementss for ductile engineered cementitious composites (ECC)." *Composites Part B: Engineering*, 184, 107741.

Zhang, M., Wu, H. J., Li, Q. M. and Huang, F. L., (2009). "Further investigation on the dynamic compressive strength enhancement of concrete-like materials based on split Hopkinson pressure bar tests. Part I: Experiments." *International Journal of Impact Engineering*, 36(12), 1327-1334.

Zhang, S., Li, V. C. and Ye, G., (2020b). "Micromechanics-guided development of a slag/fly ash-based strain-hardening geopolymer composite."

Cement and Concrete Composites, 109, 103510.

Zhong, H. and Zhang, M., (2020). "Experimental study on engineering properties of concrete reinforced with hybrid recycled tyre steel and polypropylene fibres." *Journal of Cleaner Production*, 259, 120914.

Zhong, H. and Zhang, M., (2021). "Effect of recycled tyre polymer fibre on engineering properties of sustainable strain hardening geopolymer composites." *Cement and Concrete Composites*, 122, 104167.

Zhong, H. and Zhang, M., (2022a). "Dynamic splitting tensile behaviour of engineered geopolymer composites with hybrid polyvinyl alcohol and recycled tyre polymer fibres." *Journal of Cleaner Production*, 379, 134779.

Zhong, H. and Zhang, M., (2022b). "Effect of recycled polymer fibre on dynamic compressive behaviour of engineered geopolymer composites." *Ceramics International*, 48(16), 1151-1168.

Zhong, H. and Zhang, M., (2023). "Engineered geopolymer composites: A state-of-the-art review." *Cement and Concrete Composites*, 135, 104850.

Zhong, H., Chen, M. and Zhang, M., (2023). "Effect of hybrid industrial and recycled steel fibres on static and dynamic mechanical properties of ultra-high performance concrete." *Construction and Building Materials*, 370, 130691.